Geospatial-based automated watershed modeling in Garhwal Himalaya

U. C. Kothyari, Raaj. Ramsankaran, D. Sathish Kumar, S. K. Ghosh and Nisha Mendiratta

ABSTRACT

An automated GIS tool and its computational outcomes on the spatial distribution of runoff and soil erosion are presented. The developed tool, named Automated Soil Erosion Assessment Tool (ASEAT), simulates runoff and soil erosion rates based on the concept of erosion processes suggested by Morgan–Morgan–Finney (MMF) in 1984. ASEAT is provided with a user-friendly graphical user interface (GUI) to interact with the users. The computational algorithms used are made fully automated and have been developed using the ERDAS Macro Language (EML) and Spatial Macro Language (SML). The developed modelling methodology is applied to the data of an experimental watershed of Pathri Rao in the Indian lower Himalayan region. Generated spatial distribution of runoff potential and soil erosion rates for the studied watershed using ASEAT are depicted by maps. The model-computed surface runoff potential (145.63 mm) available in the watershed seems fair when compared with the runoff depth (176.07 mm) observed at the watershed outlet. The derived estimates of soil erosion are validated, albeit qualitatively, with field observations and seem reliable for making decisions on the adoption of soil erosion conservative measures in the watershed.

Key words | GIS, Himalayan watershed, MMF modeling, remote sensing, runoff, soil erosion

U. C. Kothyari
Raaj. Ramsankaran (corresponding author)
S. K. Ghosh
Department of Civil Engineering,
Indian Institute of Technology Roorkee,
Roorkee 247 667, Uttarakhand,
India
E-mail: *ramsankaran_raaj@yahoo.co.in*

D. Sathish Kumar
Department of Hydrology,
Indian Institute of Technology Roorkee,
Roorkee 247 667, Uttarakhand,
India

Nisha Mendiratta
NRDMS Division,
Department of Science and Technology,
New Delhi 110 016,
India

INTRODUCTION

Assessment of the pattern and the amount of soil erosion is necessary to provide information needed by soil conservationists. Several computer simulation models are available for this purpose such as Universal Soil Loss Equation (USLE), which is a statistical model developed, modified and updated by Wischmeier & Smith (1978), AGNPS (Young *et al.* 1987), ANSWERS (Beasley *et al.* 1980), WEPP (Nearing *et al.* 1989) and SWAT (Arnold *et al.* 1998). Such models are becoming increasingly popular as these provide a quantitative and consistent approach for estimating rates of soil erosion for different climatic regions with a wide range of land use and management practices.

Among these models, the USLE has remained the most practical method of estimating soil erosion potential in fields and to estimate the effects of different control management practices on soil erosion for nearly 40 years (Dennis & Rorke 1999; Kinnell 2000). Although USLE has been used widely through various modified versions, its application in mountainous terrain with steep slopes is still questionable.

This equation, though universal in name, has limitations in terms of its universal application to many areas outside the United States of America. Nevertheless USLE provides a useful background in understanding the erosion process. An understanding of the development and limitations of the USLE is necessary to obtain accurate results with it. The equation can only predict a few types of erosion rates under a limited set of circumstances. It predicts inter-rill and rill erosion, but not gully, channel, stream bank or mass erosion. It was designed to model long-term erosion rates and not storm-based erosion. The accuracy of the equation

doi: 10.2166/hydro.2010.024

declines when short-term rainfall records are used. However, the process-based models like AGNPS, ANSWERS, WEPP, SWAT, etc, overcome the limitations of USLE but are much more expensive because of the need for descriptive physical details of the processes involved.

Morgan *et al.* (1984) presented a simple physically based model for predicting annual soil loss from field-sized areas on hillslopes (hereafter referred to as the MMF model). They used the concepts proposed by Meyer & Wischmeier (1969) and Kirkby (1976) to provide a stronger physical base than the USLE for erosion estimation, yet retaining the advantages of an empirical approach for process simulation and data requirement. The model was validated by the developers using erosion plot data for 67 sites in 12 countries and then applied to simulate erosion over a 100-year period in Malaysia under shifting cultivation.

Since then, due to the simplicity, flexibility and strong physical base, several researchers have used the MMF model successfully in a wide range of environments ranging from Indonesia (Besler 1987) to Nepal (Shrestha 1997) and the Rocky Mountains (Morgan 1985). De Jong & Riezebos (1992) incorporated the model into a Geographical Information Systems (GIS) from which De Jong (1994) developed SEMMED (Soil Erosion Model for Mediterranean areas) and applied it to the Bas-Vivarais area of Ardèche Province, southern France, using remote sensing as the data source. Paracchini *et al.* (1997) applied SEMMED to the 100 km^2 Timeto watershed in Sicily. Likewise studies by Ulanbek (2000), Jain *et al.* (2001), Patel *et al.* (2002), Kumar & Sharma (2005) and Ramsankaran *et al.* (2007, 2009) have been reported for the successful application of the MMF model in Indian Himalayan watersheds.

In almost all the studies reported above, researchers used the MMF concepts by utilizing separate codes for the GIS component instead of integrating the MMF concepts with a GIS system. The use of uncoupled GIS analysis involves a lot of work in exchanging the datasets, analysis and formatting the results, which in turn demands skilled manpower to do complex GIS analysis. To avoid these complications and make the analysis easy, fast and reliable, the concept of automated decision support systems was developed for different purposes. This type of GIS-driven system is popularly called Spatial Decision Support Systems (SDSS).

As no such automated tool for MMF-based soil erosion assessment has been reported in the scientific literature, an attempt has thus been made to automate the entire simulation process of the MMF model. As a result, an automated grid GIS-based tool has been developed herein and tested in soil erosion studies for the watershed of Pathri Rao, a medium-sized Himalayan watershed located at the foothills of the lower Shiwalik ranges of the Himalayas in the Garhwal region of India.

MMF (1984) MODEL

The MMF model is divided into two distinct phases of simulation, viz. the water phase and sediment phase. In the water phase, an estimation is carried out of the kinetic energy due to rainfall exerted on the soil and the volume of overland flow. Kinetic energy (E) expressed as J/m^2 can be calculated from annual rainfall (R) and the intensity (I) of the erosive rain as represented by Equation (1):

$$E = R(11.9 + 8.7 \log I) \quad (1)$$

where R is in mm and I is in mm/h. The annual overland flow (Q) in mm is calculated from the average annual rainfall, number of rain days during the year, landuse type and soil type of the area by using Equation (2):

$$Q = R \exp(-R_c/R_o) \quad (2)$$

where

$$R_c = 1000MS \times BD \times RD(E_t/E_o)^{0.5} \quad (3)$$

and MS is soil moisture content at a field capacity of 1/3 bar tension (% w/w), BD is the bulk density of the top layer (Mg/m^3), RD is topsoil root depth (m) defined as the depth of soil from the surface to the stony impermeable layer; to the base of the A-horizon, to the dominant root base or to 1.0 m, whichever is shallowest and

$$R_o = R/R_n \quad (4)$$

where $R_n =$ number of rainy days.

This sediment phase of the MMF model carries out the estimation of the sediment transport capacity of the overland flow and rate of detachment by raindrop impact. The

transport capacity due to overland flow (G) is dependent on the volume of overland flow (Q), crop cover management factor and the topography of the area and is expressed in kg/m^2 and is given by Equation (5):

$$G = 10^{-3} C Q^2 \sin(S) \quad (5)$$

where

C crop cover management factor
S steepness of land slope expressed in degrees.

The rate of soil detachment by raindrop impact (F) depends on the kinetic energy of the rainfall and soil detachability index. The rate of detachment is expressed in kg/m^2 and is given by Equation (6):

$$F = 10^{-3} K (E e^{-Aa})^b \quad (6)$$

where

K soil detachability index (g/J)
A percentage of rainfall contributing to permanent interception and stream flow
a and b are coefficients with $a = 0.05$ and $b = 1.0$.

The estimates of soil particle detachment by raindrop impact (F) are then compared with the annual transport capacity (G) and the lesser of the two values is the annual erosion rate.

AUTOMATED SOIL EROSION ASSESSMENT TOOL (ASEAT)

A GIS-based tool called Automated Soil Erosion Assessment Tool (ASEAT) is developed herein to provide an easy-to-use interface for estimating surface runoff and soil erosion rate by using the concepts of Morgan *et al.* (1984). For customising the spatial analysis module, the object-oriented languages EML (Earth Resources Data Analysis System, ERDAS Macro Language Reference Manual 2000) and SML (ERDAS Spatial Modular Language Reference Manual 2000) have been used to create the necessary graphical user interfaces. This tool works with ERDAS in the background within a Windows environment.

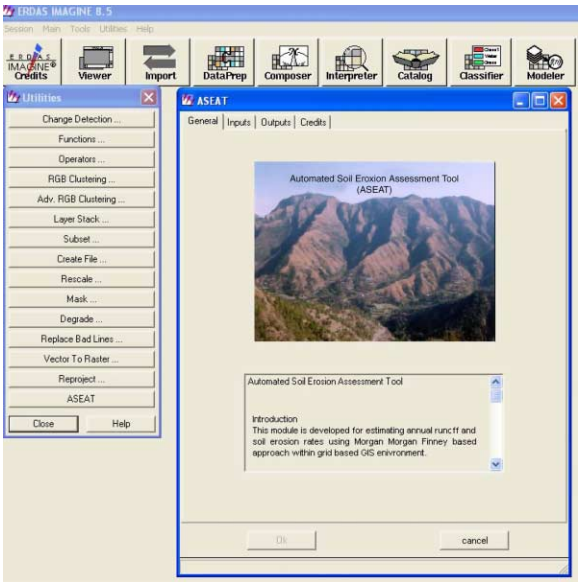

Figure 1 | GUI of the ASEAT module.

The interface consists of four tab frames and two buttons "Ok" and "Cancel" (Figure 1). The first tab frame "General" provides the general information about the interface, while the second frame "Inputs" is used for

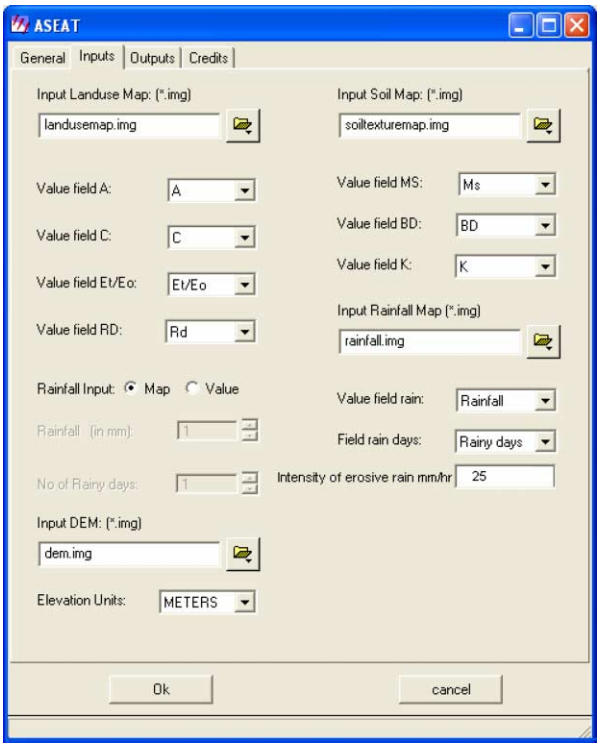

Figure 2 | GUI of the ASEAT input window.

Figure 3 | GUI of the ASEAT output window.

giving the input of the basic input layers and attribute names. Various thematic layers with necessary attributes required for modelling can be prepared either within the ERDAS environment itself or through any other GIS package and should be given as raster inputs directly to ASEAT through the graphical user interface (GUI). The third frame "Outputs" is provided for specifying the filenames of the output layers. The fourth frame "Credits" provides information on the developer's. The GUIs developed for defining input and output GIS layers are shown in Figures 2 and 3. The overall GUI consists of menus and frames to simplify the procedure and allows the user to create the required output layers by selecting appropriate check boxes and specifying output filenames. The process involved in ASEAT for runoff and soil erosion prediction is shown in Figure 4.

DESCRIPTION OF THE STUDY AREA

The Pathri Rao watershed is situated between the latitudes of 29°06′ N to 30°02′ N and longitudes of 78°00′ E to 78°06′ E and having elevations ranging from 220–730 m above the

Figure 4 | Flowchart depicting the algorithms used for soil erosion and overland flow depth prediction by the MMF–ASEAT.

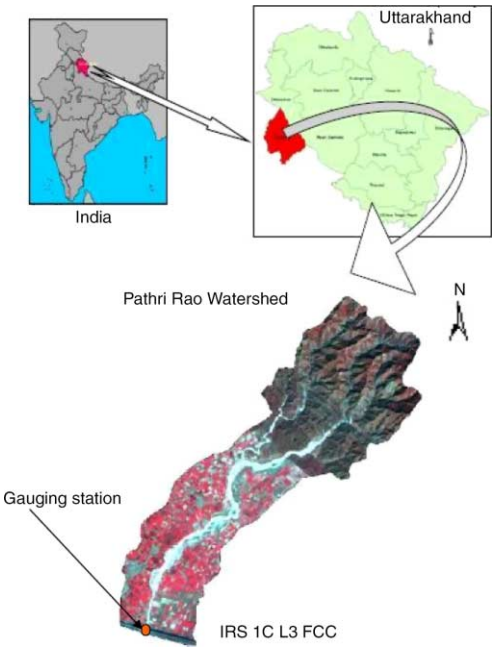

Figure 5 | Location map of the Pathri Rao watershed.

mean sea level (Figure 5). The geographical area of the watershed is 43.93 km^2. The watershed receives an average annual rainfall of 1,100 mm with an average of 50 rain days and more than 80% of the annual rainfall occurs during the monsoon season, i.e. between June to September. The mean minimum and maximum temperature in the region are 3°C and 42°C, respectively. The mean relative humidity varies from a minimum of 40% in April to a maximum of 85% in July. The overall climate of the region can be classified as semi-arid to humid subtropical. The major soil textures found in the watershed are sandy loam, loam and silt loam. The lower tracts of the watershed area have flat slopes and are therefore densely habituated while the upland areas consist of mostly hilly terrain having steep slopes. These areas are densely forested and form part of the Rajaji National Park. The dominant crops in the study area are wheat and sugarcane.

DATA AND SOFTWARE USED

In this study, different types of data have been used to extract the necessary information for use as input to the ASEAT module. These are:

(i) Indian Remote Sensing satellite (IRS) 1-C Linear Imaging Self Scanner (LISS) III of path no. 105 and row no. 55, of 11 March 2005.
(ii) Survey of India (SOI) digital topographical map at a scale of 1: 50,000 having contour interval at 20 m.
(iii) Hydro-meteorological data for the year 2005.
(iv) Digital soil map of Pathri Rao watershed

ArcGIS 9.0 and ERDAS IMAGINE 8.6 have been used for the preparation of the required database and for the analysis at various stages in preprocessing and post-processing of the spatial data. However, the automated modeling of runoff and soil erosion is implemented and coupled in the ERDAS IMAGINE software.

FIELD OBSERVATIONS

For the purposes of this study field observations have been made for the year 2005. As the hydrological response of the modelling tool would undoubtedly be governed by the quality of the inputs, a distributed approach to represent the spatial heterogeneity of the watershed characteristics and hydrological inputs has been adopted. To represent the spatial pattern of rainfall in the watershed, data from three meteorological stations, which are located inside the watershed or in its close proximity, have been utilized. The spatial locations of these rain gauges are shown by the corresponding Voronoi polygons' map (Figure 6).

The watershed was gauged at its outlet for the present study to make observations on surface runoff discharge and sediment load transport. The gauging site was installed with a manually operated stage recorder (Figure 7) to measure the depth of flow. A stable and straight river reach of about 100 m in length was selected for this purpose. The flow stage was recorded at 15 min intervals during most of the rainfall events that occurred during the period of study starting from June 2005 – September 2005. No runoffs have occurred in the river beyond the stated period. The flow velocity was measured during the periods concurrent to the observation of rainfall and river stage, by observing the time taken by a wooden float (15 × 15 × 15 cm) to cover a distance of 100 m along the flow in the river. The river cross section was measured just before commencement of the rainy season.

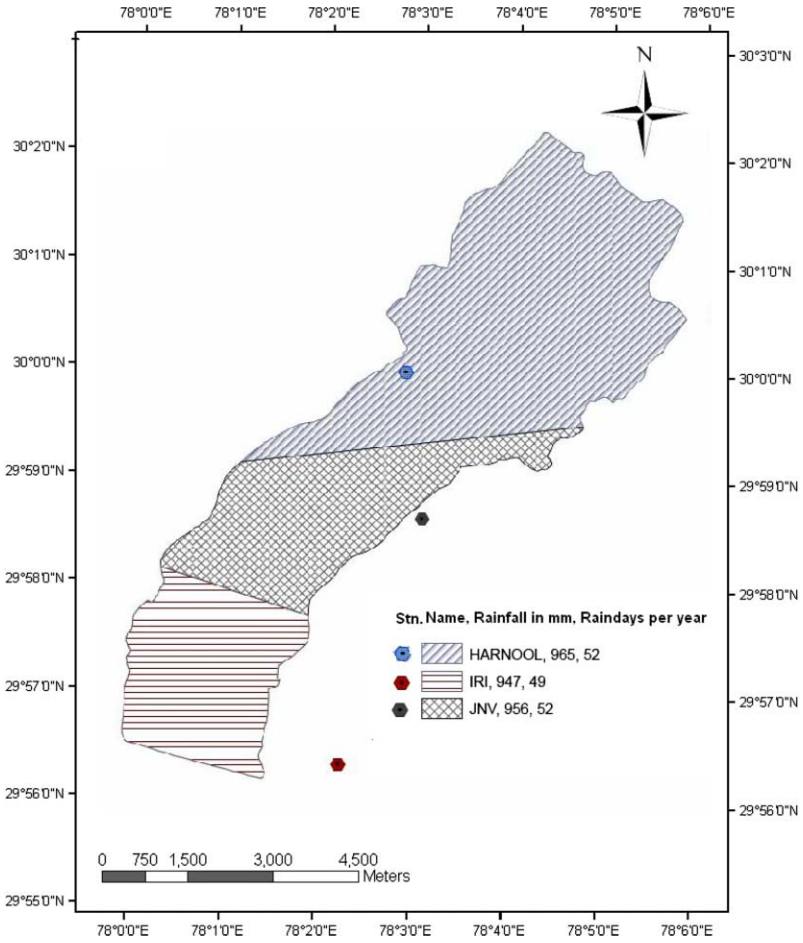

Figure 6 | Voronoi map of effective spatial extent of raingauge observations.

Based on this, the discharge flowing through the stream at the outlet was worked out.

The measurements for the sediment load at the gauging site were made by manually collecting sediment–water mixture samples at every 1 h interval using one litre cylindrical bottle sediment samplers. The dates on which the storm events were sampled are listed in Table 1. The storm events (Table 1) occurred for up to a maximum period of 14 h during any of the days. The concentration of sediment for each collected sample was determined by subsequently filtering, drying and weighing the collected samples in the laboratory. The volume of runoff (m^3) times the sediment concentration ($mg\,L^{-1}$), corrected for the units used, gave the sediment production from the rainfall events. Most of the storm events, except those which occurred during the nights,

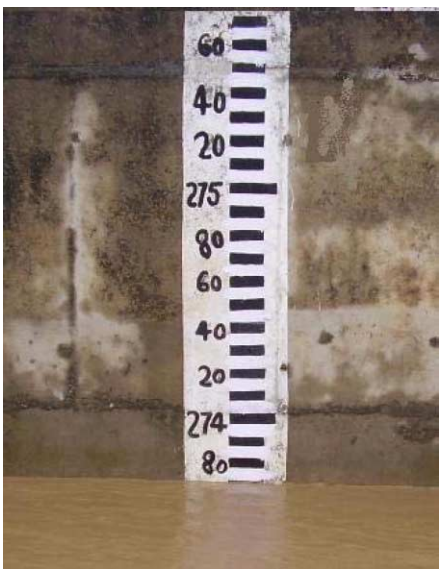

Figure 7 | Manual stage recorder at the gauging station of the Pathri Rao watershed.

Table 1 | Summary of the observed rainfall–runoff–sediment yields in the Pathri Rao watershed for the monsoon of 2005

		Rainfall depth (mm)				
S. no.	Date of storm event	Harnool station	JNV station	IRI station	Total storm runoff (mm)	Sediment yield (tonnes)
1	21.6.05	2.8	3	2.3	NIL	NIL
2	22.6.05	4.8	4.75	5.2	NA	NA
3	24.6.05	2.14	2.5	–	NIL	NIL
4	26.6.05	36.07	36	34.8	4.08	278.33
5	28.6.05	18.65	18.65	15.65	3.64	238.3
6	1.7.05	17.41	17.45	16.23	2.9	67
7	3.7.05	9.2	9.25	8.7	1.7	37
8	5.7.05	21.14	21.2	22.9	4.25	NA
9	8.7.05	12.84	12.9	11.7	2.98	NA
10	10.7.05	17.34	17.7	17.7	3.1	110
11	11.7.05	35.63	34.25	32.8	5.98	NA
12	13.7.05	58.12	57	59.3	9.55	1221
13	14.7.05	6.22	6.2	5.9	0.92	NA
14	16.7.05	17.41	15.8	16.3	2.33	58
15	17.7.05	2.24	2.1	1.7	NA	NA
16	18.7.05	21.39	22.7	20.7	3.88	484
17	20.7.05	79.43	78.2	76.4	15.3	1650
18	23.7.05	40.34	40	38.7	6.41	916.2
19	25.7.05	9.95	10.4	9.8	1.8	NA
20	26.7.05	12.98	13.5	11.3	3.66	142
21	29.7.05	7.5	7.5	8.9	NA	NA
22	30.7.05	44.27	44	44.6	8.45	1108.73
23	31.7.05	5.3	5.3	5.2	2.2	NA
24	4.8.05	39.04	39	38.9	5.85	731.18
25	5.8.05	6.42	6.4	5.7	3.02	97.8
26	6.8.05	24.87	24.8	26.1	5.12	744.80
27	8.8.05	17.41	16.5	15.7	4.5	556
28	13.8.05	11.94	10.7	11.2	2.1	46.3
29	16.8.05	34.87	35.5	37.8	NA	NA
30	17.8.05	12	12.3	12	4.19	748
31	21.8.05	8.43	7.8	7.9	1.05	29.6
32	24.8.05	19.8	19.8	21.6	NA	NA
33	26.8.05	3.5	3.7	2.6	NIL	NIL
34	29.8.05	5.2	4.8	5.5	NA	NA
35	30.8.05	6.7	6.3	6.3	1.36	30.2
36	1.9.05	7.9	7.7	8.7	2.25	52.9
37	4.9.05	1.83	1.5	2.2	NIL	NIL
38	5.9.05	15.1	15.1	12.9	3.97	519
39	10.9.05	17.93	18.5	22.5	2.36	113.61
40	12.9.05	7.21	6.8	8.2	2.2	44
41	14.9.05	5.97	5.5	5.5	1.47	31
42	15.9.05	1.74	1.4	–	NIL	NIL
43	16.9.05	2.74	2.3	2.7	NIL	NIL
44	18.9.05	73.49	72.6	72.4	16.42	1986
45	20.9.05	2.1	2.1	–	NIL	NIL
46	23.9.05	29.87	29.1	27	6.43	732
47	24.9.05	90.43	89.7	91.5	21.05	2791.4

Table 1 | (*continued*)

S. no.	Date of storm event	Rainfall depth (mm) Harnool station	JNV station	IRI station	Total storm runoff (mm)	Sediment yield (tonnes)
48	25.9.05	4.97	5.5	8.5	3.8	137
49	26.9.05	10.28	9.85	9	3.25	98
50	27.9.05	9.44	9.4	8.9	2.55	64.8
51	28.9.05	8.9	8.5	7.6	NA	NA
52	30.9.05	1.87	2.4	1.8	NIL	NIL
	Annual values	965.12	955.9	947.48	176.07	15814.8

Note: NA – Not Available; Nil – No runoff generated.

were gauged by camping at the project site during June 2005–September 2005.

In the year 2005 this region received about 90% of the yearly rainfall during the monsoon months of June to September. Only a few rainfall events occurred over the study area without generating any runoff during the winter and summer months of the year 2005. In summing up, there were 52 rainfall events which occurred during the monsoon of 2005. Only 44 rainfall events produced runoff and most of those were observed by us through

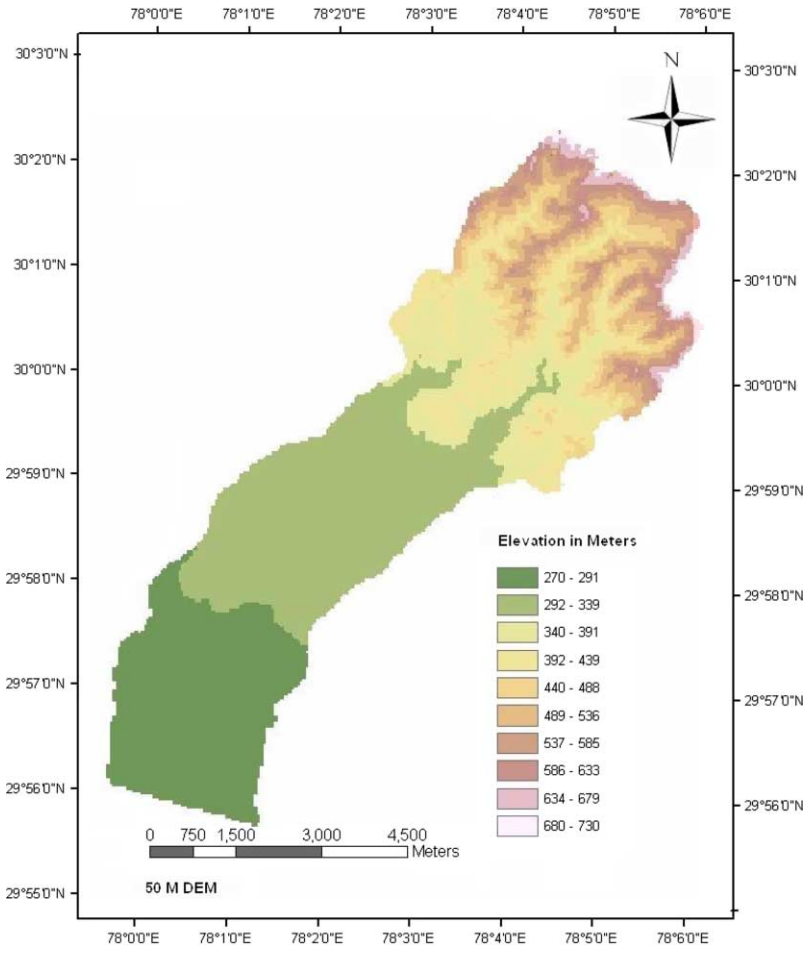

Figure 8 | Digital Elevation Model of the Pathri Rao watershed.

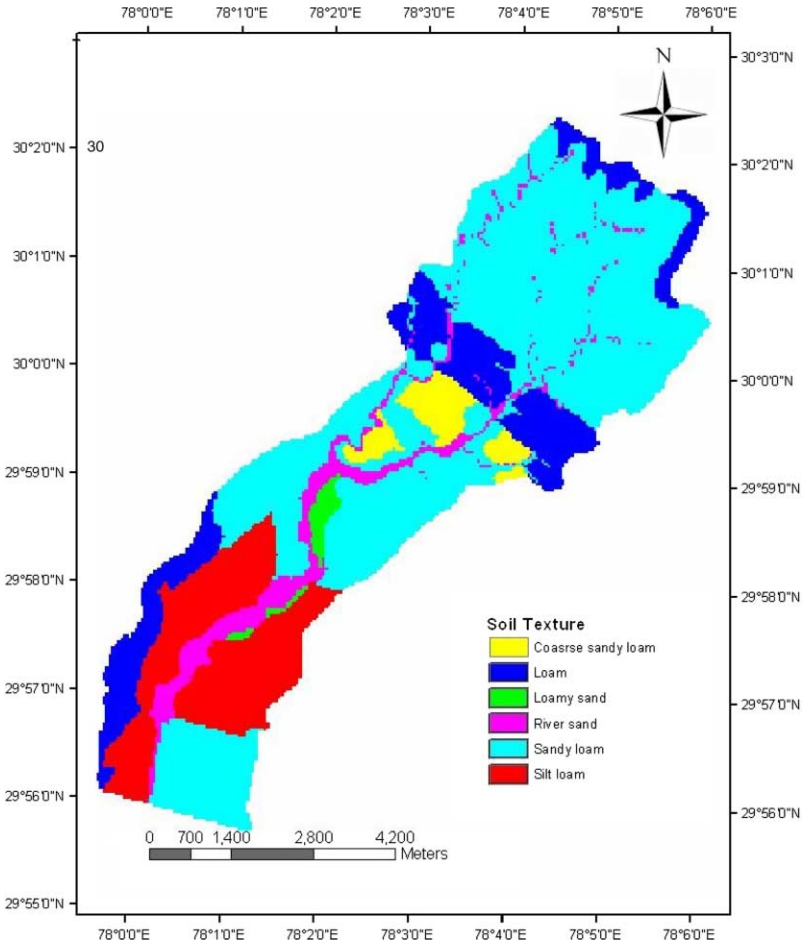

Figure 9 | Soil texture map of the Pathri Rao watershed.

intensive field campaigns (Kothyari & Ramsankaran 2010). The sediment production rate from these observed storm events was determined by using currently made observations. Summarized data from the field observations on the date of the storm event, rainfall, runoff and sediment yield are given in Table 1. The annual values of these variables are also worked out in Table 1, given that about 85% of the rainfall–runoff events occurred during the observed period measured. Further, the annual rate of sediment production as determined by summing up the sediment production rates for the individual storm rainfall events measured during the year was divided by the watershed area to produce the annual sediment yield expressed as tonnes per hectare.

Table 2 | Different soil units and modeling parameters*

Soil texture	*MS*	*BD*	*K*
River sand	0.08	1.5	1.2
Loam	0.2	1.3	0.8
Sandy loam	0.28	1.2	0.7
Loamy sand	0	0	0.3
Coarse sandy loam	0.28	1.2	0.7
Silt loam	0.25	1.3	0.9

*MS: soil moisture content at field capacity 1/3 bar tension (% w/w), BD: bulk density of top layer (Mg/m^3), K: soil detachability index (g/J).

GENERATION OF INPUTS

The proposed interface for the MMF model uses six operating functions, for which 15 parameters are required. All these could be generated from various datasets through the use of documented procedures as explained below.

The watershed boundary was extracted from the Survey of India (SOI) topographical maps at a scale of 1:50 000

Table 3 | Tasseled cap coefficients for LISS II sensor (Sharma *et al.* 1990)

	Greenness coefficients	
Band	**IRS LISS II A**	**IRS LISS II B**
1	−0.1264	−0.1072
2	−0.1240	−0.1219
3	−0.4382	−0.4341
4	−0.8813	−0.8861

having contour intervals at 20 m and stored within the GIS environment as a polygon map. Next a 50 × 50 m Digital Elevation Model (DEM) of the watershed was generated using contour interpolation techniques available in ArcGIS (Figure 8). A soil texture map of the studied watershed (Figure 9) was procured from the Agriculture and Soils Division, Indian Institute of Remote Sensing, Dehradun, India (IIRS) to derive the various parameters like soil detachability index (*K*), soil moisture content at field capacity (*MS*) and bulk density of top layer (*BD*) based on different textures of the soil as per Morgan (1995) (Table 2).

In the present study, cloud-free digital data from IRS-1C LISS-III has been used for extracting landuse information. Initially, the satellite data has been registered with the base map of the area by matching prominent identifiable features such as road crossings, canals, bridges, etc, on both the base

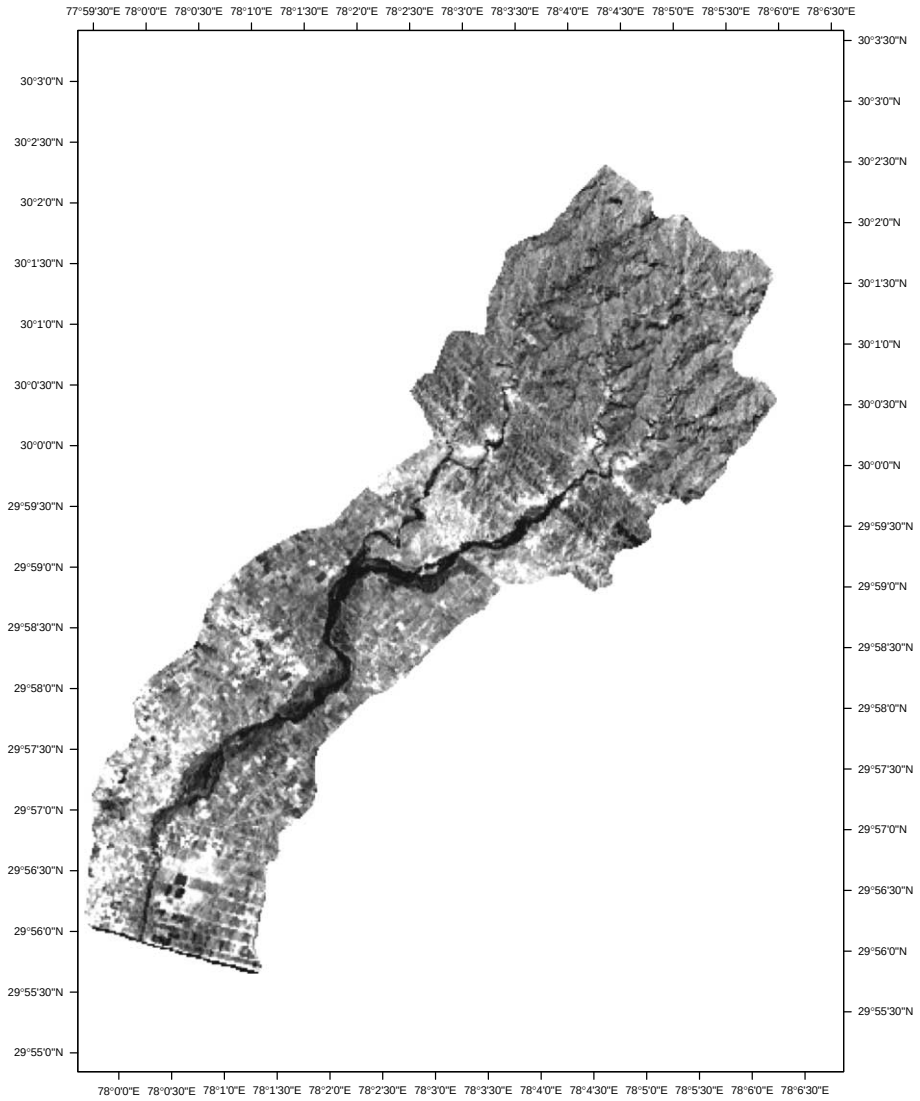

Figure 10 | TC greenness image of the LISS III scene of the Pathri Rao watershed.

map as well as on the satellite data. Efforts were made to ensure that the ground control points (GCP) are uniformly distributed on the image. A second-order polynomial model was generated with a RMS error of less than a half a pixel. Subsequently, the watershed area on the geo-coded satellite scene has been extracted by overlaying the boundaries of the watershed as delineated from the digital topographical map.

Satellite data can be transformed or manipulated in several ways so that certain typical information can be highlighted while the rest is masked out. Some of the techniques used for such purposes are image division, commonly known as image ratio, Normalized Difference Vegetation Index (NDVI), Tassel Cap transformation (TC), Principal Component Analysis (PCA), etc. Detailed descriptions of these techniques are given by Jensen (1996, 2000) and Schowengerdt (1997), amongst others. Ghosh (1991) used these techniques along with the original data to classify landuse for the Scottish Basin and used its output as input into the SWM4 model. It was observed that nearly 26% improvement in classification accuracy could be achieved by including these transformed datasets along with the original data. Hence the same approach, i.e. using the original satellite data along with synthetically generated data (such as TC and PCA extracted from the original data),

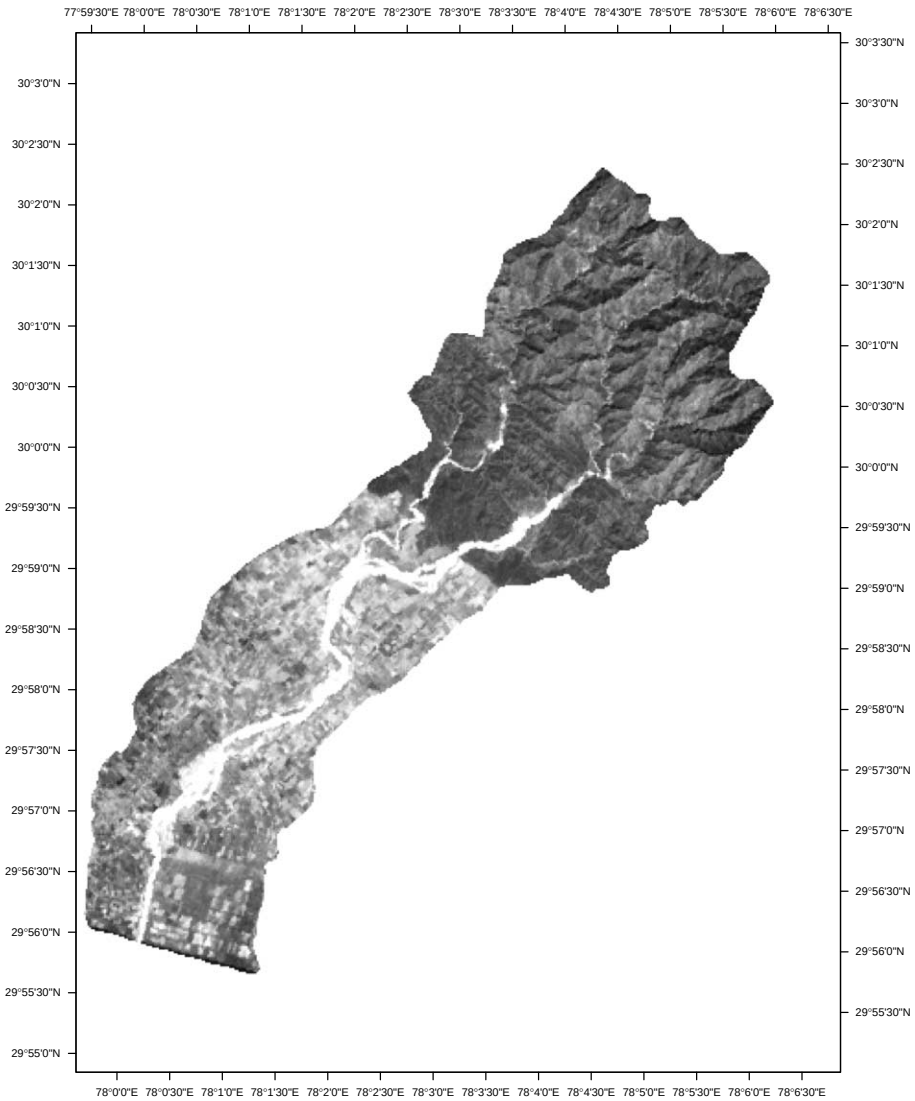

Figure 11 | First component PCA image of the LISS III scene of the Pathri Rao watershed.

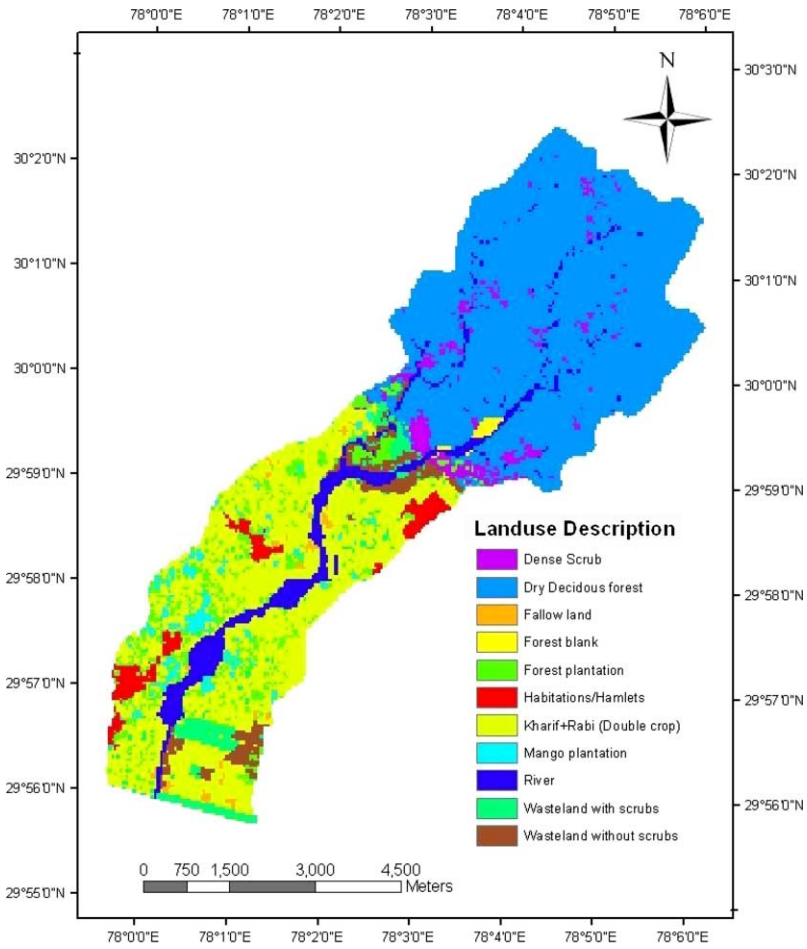

Figure 12 | Landuse/cover map of the Pathri Rao watershed.

is used in the present study for classifying land use and land cover.

For the purpose of generating TC and PCA images, all the bands of the above-mentioned IRS LISS III image have been used. Since the TC coefficients for LISS III are not available, LISS II TC coefficients have been used (Table 3) to generate a greenness image. The resultant TC greenness image (Figure 10) displays areas with healthy, green vegetation as the brightest feature and also it reveals the spatial pattern of green vegetation to some extent and thus would help to separate vegetation from bare features during the classification process. Similarly, Principal Components Analysis on the IRS LISS III image has been carried and it is found that the majority of the information contained in all three bands of the IRS LISS III data can be explained by the first component of PCA. Thus, the first component image of PCA was used in place of all four original bands without much loss of information. Subsequently, the first three bands of the geometrically corrected IRS 1C LISS III image are merged with the TC greenness image and the first component PCA image (Figure 11) to form a layered synthetic image using the layer stacking algorithm in ERDAS IMAGINE. Thus a synthetic image is formed having the following layers, where layer 1 contains the PCA–I image, layer 2 has the TC greenness image, layer 3 has LISS III band 2, layer 4 has LISS III band 3 and layer 5 has LISS III band 4. Subsequently a prepared synthetic image which is free from redundant information has been classified for generating land use/cover for the study area by the maximum likelihood classifier algorithm in ERDAS IMAGINE-8.6. The accuracy of the prepared digital landuse map (Figure 12) is 84%. The detailed statistics of

Table 4 | Landuse classification error matrix

	Reference data										
Classified data	**1**	**2**	**3**	**4**	**5**	**6**	**7**	**8**	**9**	**10**	**11**
1	34	0	8	0	0	0	0	0	0	0	0
2	0	31	0	0	2	2	0	0	0	0	0
3	6	6	62	0	0	0	1	0	0	0	0
4	0	0	0	22	0	0	6	2	0	0	0
5	0	1	0	0	49	5	3	0	0	0	0
6	0	1	0	0	2	56	2	2	0	0	0
7	0	0	0	3	0	2	55	13	0	0	2
8	0	0	0	0	1	3	10	121	0	1	0
9	1	2	0	0	0	0	0	0	17	0	0
10	0	0	0	0	0	0	0	4	0	33	0
11	0	0	0	0	0	4	2	0	0	0	38
Column total	41	41	70	25	54	72	79	142	17	34	40

1 – dense scrub, 2 – river, 3 – dry deciduous forest, 4 – mango plantation, 5 – wastelands without scrubs, 6 – wastelands with scrubs, 7 – forest plantation, 8 – Kharif + Rabi (double crop), 9 – forest blanks, 10 – fallow land, 11 – habitations/hamlets.

the obtained accuracy are also given in Tables 4–6. For the landuse classes as shown in Figure 12, parameters like percentage of rainfall contributing to permanent interception and stream flow (A), top soil root depth in meters (R_d), crop cover management factor (C) and ratio of actual (E_t) to potential (E_o) evapotranspiration E_t/E_o are assigned to individual cells according to the plant growth stage (Table 7) as suggested by Morgan *et al.* (1984). The rainfall for the simulation year is provided in a spatially distributed manner by considering the rainfall observed at three stations for deriving R, R_o and R_n values for each grid cell (Figure 6). The complete procedure adopted for extracting and generating the above-mentioned input parameters is depicted in Figure 13, which is self-explanatory.

SIMULATION METHODOLOGY

The digital layers of the spatially distributed thematic map of DEM, landuse, soil and rainfall containing the attributes

Table 5 | Landuse classification accuracy totals

Landuse categories	**Reference total**	**Classified total**	**Number correct**	**Producer's accuracy (%)**	**User's accuracy (%)**
Dense scrub	41	42	34	82.93	80.95
River	41	35	31	75.61	88.57
Dry deciduous forest	70	75	62	88.57	82.67
Mango plantation	25	30	22	88.00	73.33
Wasteland without scrubs	54	58	49	90.74	84.48
Wasteland with scrubs	72	63	56	77.78	88.89
Forest plantation	79	75	55	69.62	73.33
Kharif + Rabi (double crop)	142	136	121	85.21	88.97
Forest blank	17	20	17	100.00	85.00
Fallow land	34	37	33	97.06	89.19
Habitations/hamlets	40	44	38	95.00	86.36
Totals	615	615	518		

Table 6 | Landuse classification kappa statistics

Landuse categories	Kappa
Dense scrub	0.7959
River	0.8776
Dry deciduous forest	0.8044
Mango plantation	0.722
Wasteland without scrubs	0.8299
Wasteland with scrubs	0.8742
Forest plantation	0.694
Kharif + Rabi (double crop)	0.8566
Forest blank	0.8457
Fallow land	0.8856
Habitations/hamlets	0.8542
Overall kappa statistics	0.8208

Table 7 | Different landuse and modeling parameters*

Landuse categories	A	C	E_t/E_o	R_d
Dense scrub	25	0.1	0.8	0.05
River	0	0	0	0
Dry deciduous forest	30	0.002	0.92	0.1
Mango plantation	25	0.2	0.85	0.1
Wasteland without scrubs	0	1	0.05	0.02
Wasteland with scrubs	15	0.01	0.1	0.05
Forest plantation	25	0.01	0.8	0.05
Kharif + Rabi (double crop)	30	0.2	0.75	0.07
Forest blank	15	1	0.1	0.05
Fallow land	10	0.2	0.58	0.05
Habitations/hamlets	10	0	0	0

*A – percentage of rainfall contributing to permanent interception and stream flow, C – crop cover management factor, E_t/E_o – ratio of actual (E_t) to potential (E_o) evapotranspiration, R_d – top soil root depth in meters.

for S, A, R_d, C, E_t/E_o, K, MS and BD are provided as raster inputs to the soil erosion prediction module ASEAT in ERDAS IMAGINE. Morgan *et al.* (1984) has suggested that 25 mm/h rainfall intensity be taken as the erosive rainfall to initialize the model run. Then, to estimate the soil erosion due to splash detachment, the corresponding computed sediment transport capacity of the overland flow and rate of soil detachment are compared internally and, if the transport capacity is greater than the rate of soil detachment, the soil detachment value is adopted as the soil loss value. Similarly, if the rate of soil detachment is higher than the transport capacity of overland flow, then the value of transport capacity is adopted as the soil loss value. The spatial model then analyzes each pixel in the given attribute layers. Based on the output value of erosion

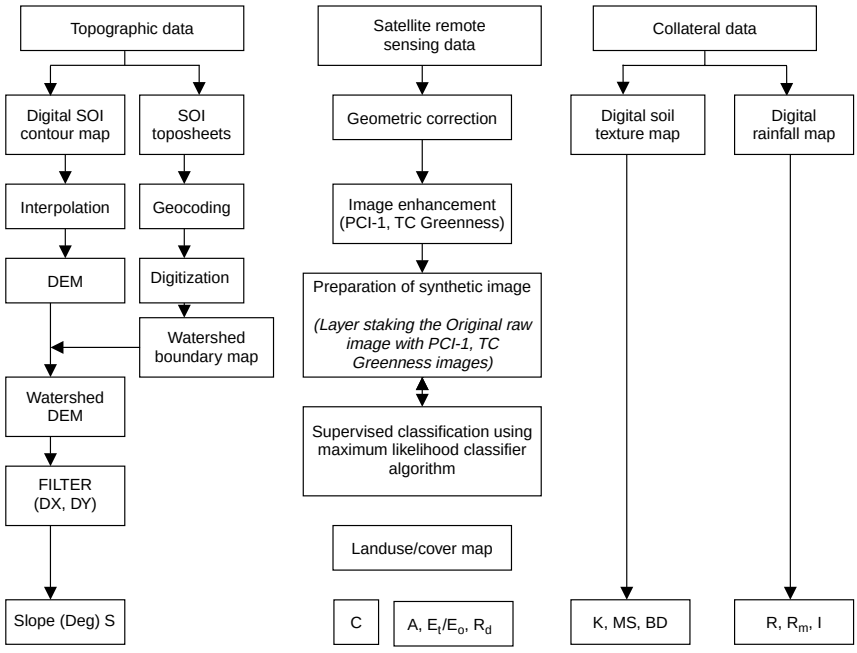

Figure 13 | Flowchart for extracting and generating input parameters to the soil erosion model.

for each pixel, the minimum value in the output layer is taken as the erosion rate of that particular pixel and similarly for the whole study area. As already mentioned, the complete procedure is made fully automated using EML and SML tools available within the ERDAS IMAGINE software.

RESULTS AND DISCUSSIONS

The derived pixel-based magnitude and spatial distribution of overland runoff potential and soil erosion rates in the Pathri Rao watershed are shown respectively in Figures 14 and 15. The estimated overland flow (surface runoff) potential available in the watershed is 6,398,954 m^3/yr, which indicates that more than 80% of the precipitation was infiltrated into the ground. Due to the low surface runoff potential, the availability of water becomes a crucial factor for drinking and agricultural production in the downstream region of the watershed, particularly during the summer months when rain normally does not occur. In the absence of other information a comparison between the computed surface runoff potential of the watershed with the total runoff from the watershed observed at its outlet is made and given in Table 8, which seems realistic consider-

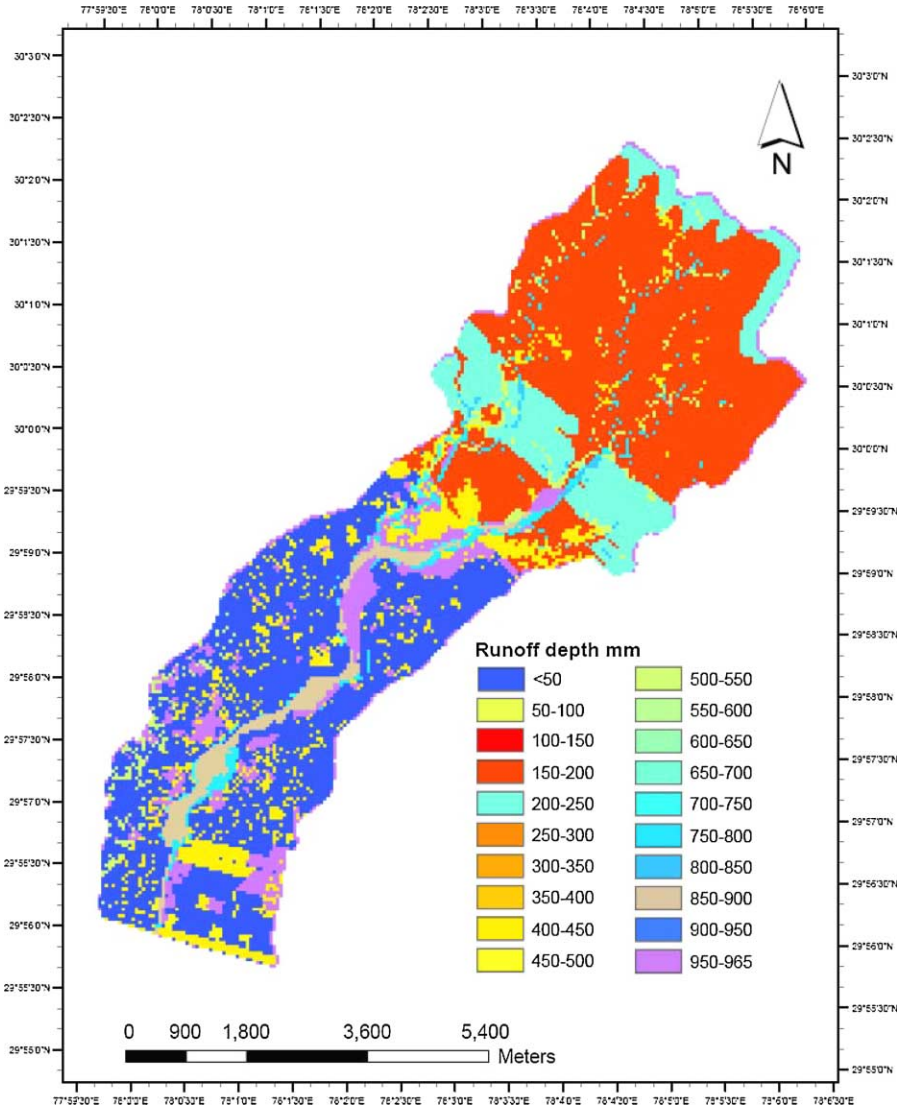

Figure 14 | Spatial distribution of potential overland flow depth for the Pathri Rao watershed.

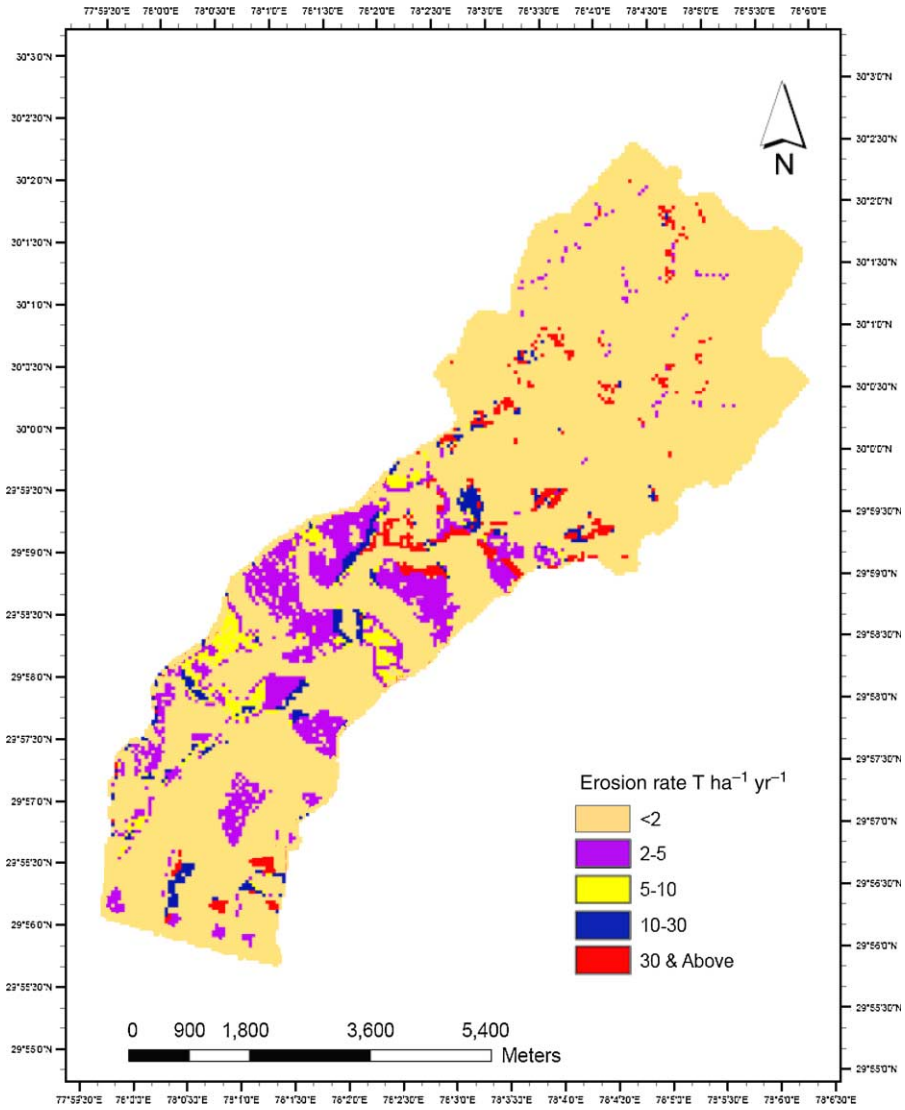

Figure 15 | Spatial distribution of potential soil erosion rate for the Pathri Rao watershed.

ing the small amount of infiltration loss that may occur till all the generated surface runoff reaches the watershed outlet. This is convincing since the catchment area of the watershed is small ($\sim$43.93 km^2) and hence routing effects on the runoff would be small. However, there is a need to further improve the MMF model to also simulate the process of surface runoff routing through the watershed. Similarly, the model estimated average annual soil erosion rate of 11.47 t ha^{-1} within the watershed appears to be reasonable. While the annual sediment yield observed through the present study at the watershed outlet is 3.6 t ha^{-1}, considering the complex natural process involving soil detachment, transport and deposition within the watershed, the value estimated by the MMF approach compared favorably with observations.

The generated spatial digital soil erosion maps give an approximation of sediment source areas and spatial distribution of soil erosion intensity. Nevertheless, it does not represent sediment yields from the cells or the watershed. It is important though to validate the accuracy of the predicted rates of soil erosion to ensure the predictive accuracy of the model and to demonstrate to

Table 8 | Comparison of the observed runoff depth and the computed surface runoff potential

Simulation year	Observed runoff depth (mm)	Computed surface runoff potential (mm)
2005	176.07	145.63

Table 9 | Area under different classes of soil erosion in Pathri Rao watershed

Soil erosion rate (t/ha/yr)	Class	Area (ha)	Percentage area
<2	None–very slight (I)	3499.5	79.65
2–5	Slight (II)	471.5	10.73
5–10	Moderate (III)	119.25	2.71
10–30	High (IV)	106.75	2.43
30 and above	Severe (V)	196.75	4.48

potential users so that definite decisions can be made based on such estimates. However, due to the lack of ground observations on the spatial distribution of soil erosion, it has not been possible herein to provide such a validation. The model outcomes are therefore verified qualitatively by georeferenced field checking and through expert knowledge-based analysis by considering the prevailing landuse type, topography, existing management practices and the literature-based estimates such as those suggested by Garde & Kothyari (1987) for the lower Himalayan watersheds. Based on these checks it is concluded that the MMF–ASEAT produced realistic values of the soil erosion estimates and its spatial distribution pattern too. The fact is that the soil erosion in this watershed is more based on the transport process due to the ephemeral nature of runoff. Thus a limiting condition exists on the transport of sediments for large distances, and hence the scenarios such as the present one may favour the applicability of the present model. Even though in quantitative terms the soil erosion rates obtained in this assessment may not be very precise, the model outputs can still be used to identify the soil erosion-prone areas with a high level of confidence.

Based on the soil erosion rates, as per Morgan (1995), areas within the watershed are presently classified as slight, moderate, high and severe erosion potential zones as listed in Table 9. An inter-comparison between the distributed vales of soil erosion rates, DEM and landuse indicated that the areas of high soil erosion belong to undulating topography and uncultivated slopes. Table 9 also indicated that about 79% of the watershed area belongs to the no or very slight soil erosion category.

It is recommended that the zones of high and severe erosion potential be given immediate attention for their treatment by soil conservationists. The alterations made, if any, in the existing landuse pattern shall result in large changes in the production of soil loss. The rates of soil erosion shall increase in the case that forested land is converted into agricultural land to meet the demand for food for a growing population.

SOIL LOSS PER LANDUSE TYPE

The rates of soil erosion are compared within the different landuse categories by superimposing the map of soil erosion rate over the landuse map in the GIS environment (Tables 10 and 11). It is observed that soil loss from the dry deciduous forest, forest plantation and hamlets are the

Table 10 | Matrix of the aerial extent (ha) of different landuse types under different erosion rates

	Landuse categories (ha)*											
Erosion class	1	2	3	4	5	6	7	8	9	10	11	Subtotal
I	5	272.75	2027.25	64.5	34.25	108.75	232.75	634.75	2.25	7.5	109.75	3499.5
II	19	0	19.25	18	1.25	11.25	1	389.5	0.25	12	0	471.5
III	6.5	0	0.25	0.25	2.75	0.25	0.25	101.75	0.25	7	0	119.25
IV	31.75	0	0	0	18.75	0	10.25	42.75	1	2.25	0	106.75
V	58.75	0	0	3.25	66.25	12.25	0	46	10	0.25	0	196.75
Subtotal	121	272.75	2046.75	86	123.25	132.5	244.25	1214.75	13.75	29	109.75	4393.75

*1 – dense scrub, 2 – river, 3 – dry deciduous forest, 4 – mango plantation, 5 – wastelands without scrubs, 6 – wastelands with scrubs, 7 – forest plantation, 8 – Kharif + Rabi (double crop), 9 – forest blanks, 10 – fallow land, 11 – habitations/hamlets.

Table 11 | Average soil loss from different landuse categories

Landuse categories	Average annual soil loss (y/ha/yr)
Dense scrub	108.16
River	0.00
Dry deciduous forest	0.37
Mango plantation	6.30
Wasteland without scrubs	169.7
Wasteland with scrubs	18.82
Forest plantation	3.9
Kharif + Rabi (double crop)	8.2
Forest blank	144.38
Fallow land	17.03
Habitations/hamlets	0.01

least. Areas under cultivation and mango plantations are prone to moderate soil loss. The areas under fallow and wastelands with scrubs are prone to a high rate of soil loss owing to the poor vegetative cover and shallow root zone. It is also observed that the areas under wasteland without scrub, consisting of fine silt and fine sand, are also prone to severe soil loss. This may be true because this landuse may have no or little vegetative cover, which induces more erosion due to direct rainfall impact and direct runoff. The dense scrubs over steep slopes are prone to severe rates of soil erosion as well. The model computations also revealed that more than 50% of the areas under dense scrub prone to severe rates of soil erosion are lying along the steep slopes. The soil erosion rates for the areas with dense scrub landuse but lying on the mild slopes have lower rates of soil erosion. It is also observed that the forest-covered area along the steep slopes has an average annual soil loss of about 144.8 $t\,ha^{-1}$ indicating the high rate of soil erosion. This may be the reason for high soil loss in these forest areas. The steeply forested slopes of the Pathri Rao watershed only support tall trees and do not sustain low height vegetation cover.

CONCLUSIONS

Observations have been made in the lower Himalayan watershed of Pathri Rao to determine the rates of overland flow potential and soil erosion during the monsoon months of the year 2005. The capabilities of the MMF model and the developed GIS tool for predicting the spatial distribution of the rate of soil erosion are demonstrated with respect to the Pathri Rao watershed. The GUI-based GIS platform used has provided a quicker method for spatial modelling and produced output maps that can be easily understood. Soil erosion estimation using the MMF model with the GIS, viz. ASEAT, allows for complete use of the vast amounts of data that can be easily assimilated and analyzed. The ease with which spatial and attributive data/information can be handled in ASEAT allows for rapid assessment of the numerous potential conservation scenarios. Thus the developed ASEAT is a valuable tool for land managers as it can be used in assessing the performance of different techniques of soil conservation at different levels of scale.

The model is found to produce realistic estimates of the spatial distribution of the overland flow potential and rates of soil erosion in the watershed of Pathri Rao. The distribution of soil erosion for different landuse types indicated that wasteland without any scrub to be the most erosion-prone, with deciduous forested land to be the least prone to soil erosion.

ACKNOWLEDGEMENTS

The authors would like to express thanks to the anonymous reviewers for contributing insightful comments and useful suggestions, which have greatly improved the quality of the present work.

REFERENCES

Arnold, J. G., Srinivasan, R., Muttiah, R. S. & Williams, J. R. 1998 Large area hydrologic modeling and assessment part I: model development. *J. AWRA* **34** (1), 73–89.

Beasley, D. B., Huggins, L. F. & Monke, E. J. 1980 ANSWERS: a model for watershed planning. *Trans. Am. Soc. Agric. Eng.* **23**, 938–944.

Besler, H. 1987 Slope properties, slope processes and soil erosion risk in the tropical rain forest of Kalimantan Timur, Indonesian Borneo. *Earth Surf. Process. Landforms* **12**, 195–204.

De Jong, S. M. 1994 Applications of reflective remote sensing for land degradation studies in a Mediterranean environment. *Nederl. Geograf. Stud.* KNAG, Utrecht.

De Jong, S. M. & Riezebos, H. Th. 1992 *Assessment of Erosion Risk Using Multitemporal Remote Sensing Data and An Empirical Erosion Model*. Department of Physical Geography, University of Utrecht, The Netherlands, Research report.

Dennis, M. F. & Rorke, M. F. 1999 The relationship of soil loss by interill erosion to slope gradient. *Catena* **38**, 211–222.

ERDAS Macro Language Reference Manual 2000 ERDAS IMAGINE V8.5, ERDAS Inc, Atlanta, GA.

ERDAS Spatial Modeler Language Reference Manual 2000 ERDAS IMAGINE V8.5, ERDAS Inc, Atlanta, GA.

Garde, R. J. & Kothyari, U. C. 1987 Sediment yield estimation. *J. Irrig. Power (India)* **44** (3), 97–123.

Ghosh, S. K. 1991 *River Basin Management using Remote Sensing Data Analysis–An Assessment of Data to Hydrological Model As derived From Satellite Data*. PhD Thesis (unpublished), University of Strathclyde, Glasgow.

Jain, S. K., Kumar, S. & Varghese, J. 2001 Estimation of soil erosion for a Himalayan watershed using a GIS technique. *Water Res. Manage.* **15**, 41–54.

Jensen, J. R. 1996 *Introductory Digital Image Processing: A Remote Sensing Perspective*, 2nd edition.. Prentice-Hall, Englewood Cliffs, NJ.

Jensen, J. R. 2000 *Remote Sensing of Environment: An Earth Resource Perspective*. Prentice-Hall, Englewood Cliffs, NJ.

Kinnell, P. I. A. 2000 AGNPS-UM: applying the USLE-M within the agricultural nonpoint source pollution model. *Environ. Modell. Softw.* **15**, 331–341.

Kirkby, M. J. 1976 Hydrological slope models: the influence of climate. In *Geomorphology and Climate* (ed. in E. Derbyshire), pp. 247–267. Wiley, Chichester.

Kothyari, U. C. & Ramsankaran, R. 2010 *Application of Distributed Hydrologic Modeling in Pathri Rao and Khulgad Watershed for Watershed Evaluation, Runoff Harnessing and Soil Erosion Abatement*. Final Project Report Submitted to NRDMS Division, Department of Science and Technology (DST) New Delhi.

Kumar, S. & Sharma, S. 2005 Soil erosion risk assessment based on MMF model using remote sensing and GIS. *Hydrol. J.* **28** (1&2), 47–58.

Meyer, L. D. & Wischmeier, W. H. 1969 Mathematical simulation of the process of soil erosion by water. *Trans. Am. Soc. Agric. Eng.* **12**, 754–762.

Morgan, R. P. C. 1985 The impact of recreation on mountain soils: towards a predictive model for soil erosion. In *The Ecological Impacts of Outdoor Recreation on Mountain Areas in Europe and North America* (ed. in N. G. Bayfield & G. C. Barrow), Vol. 9, pp. 112–121, Rural Ecology Research Group Report.

Morgan, R. P. C. 1995 *Soil Erosion and Conservation*. Longmans, Guildford.

Morgan, R. P. C., Morgan, D. D. V. & Finney, H. J. 1984 A predictive model for the assessment for the soil erosion risk. *J. Agric. Eng. Res.* **30**, 245–253.

Nearing, M. A., Foster, G. R., Lane, L. J. & Finkner, S. C. 1989 A process-based soil erosion model for USDA-Water Erosion Prediction Project technology. *Trans. Am. Soc. Agric. Eng.* **32**, 1587–1593.

Paracchini, M. L., Minacapilli, M., Bertolo, F. & Folving, S. 1997 Soil erosion modelling and coastal dynamics: a case study from Sicily. In *Remote Sensing Society: Observations and Interactions*, pp. 334–339. Remote Sensing Society, Nottingham.

Patel, N. R., Suresh Kumar, Prasad J. & Pande, L. M. 2002 Soil erosion risk assessment and land use adjustment for soil conservation planning using remote sensing and GIS. *Asian J. Geoinf.* **1** (2), 47–55.

Ramsankaran, R., Kothyari, U. C., Dasgupta, S., Rawat, J. S. & Sathish Kumar, D. 2007 Soil erosion modeling in Himalayan watershed. *Geospat. Today J.* **6** (3), 18–23.

Ramsankaran, R., Kothyari, U. C., Ghosh, S. K. & Murugesan, K. 2009 Geospatial based hydrological modeling–a pilot study in Pathri Rao watershed. *Current Science*, Manuscript submitted for publication.

Schowengerdt, R. A. 1997 *Remote Sensing: Models and Methods for Image Processing*, 2nd edition. Academic, New York.

Sharma, S. A., Bhatt, H. P. & Ajai, 1990 Generation of brightness and greenness transformations for IRS-LISS II Data. *Photonirvachak J. Indian Soc. Remote Sensing* **18** (3), 25–31.

Shrestha, D. P. 1997 Assessment of soil erosion in the Nepalese Himalaya: a case study in Likhu Khola Valley, Middle Mountain Region. *Land Husbandry* **2** (1), 59–80.

Ulanbek, T. 2000 *Soil Erosion Modeling Using Remote Sensing and GIS*. Indian Institute of Remote Sensing (IIRS), Dehradun, Project report.

Wischmeier, W. H. & Smith, D. D. 1978 *Predicting Rainfall Erosion Losses–A Guide to Conservation Planning*. US Department of Agriculture, Agricultural Handbook. USDA, Washington, DC.

Young, R., Onstad, C. A., Bosch, D. D. & Anderson, W. P. 1987 *AGNPS: Agricultural Non-Point Source Pollution Model: A Watershed Analysis Tool*. USDA, Washington, DC, USDA-Agricultural Research Service. Conservation Research Report 35.

First received 24 March 2008; accepted in revised form 22 June 2009. Available online 28 January 2010